Cellular and Molecular Bioengineering, Vol. 15, No. 5, October 2022 *(© 2022)* pp. 355–366
https://doi.org/10.1007/s12195-022-00727-x

2022 CMBE Young Innovators

High-Density Branched PEGylation for Nanoparticle Drug Delivery

Devorah Cahn[1] and Gregg A. Duncan[1,2]

[1]Fischell Department of Bioengineering, University of Maryland, College Park, MD 20742, USA; and [2]Biophysics Program, University of Maryland, College Park, MD 20742, USA

(Received 3 March 2022; accepted 15 June 2022; published online 5 July 2022)

Associate Editor Michael R. King oversaw the review of this article.

Abstract

Introduction—The surface modification of nanoparticles (NP) with a dense layer of polyethylene glycol (PEG) has been widely used to improve NP circulation time, bioavailability, and diffusion through biological barriers [e.g. extracellular matrix (ECM), mucus]. While linear PEG coatings are commonly used, branched PEG coatings have not been widely explored as a design parameter for NP drug delivery systems.

Methods—NPs were densely coated with either linear 2, 5, 10 kDa linear PEG or with 10 kDa star-shaped, 4-arm branched PEG. NP cellular uptake was evaluated in HEK-293T and A549 cells. NP stability was evaluated in fetal bovine serum over 24 h using dynamic light scattering. Diffusion of NPs within a Matrigel ECM model and sputum (mucus) collected from individuals with cystic fibrosis (CF) lung disease were analyzed through multiple particle tracking.

Results—PEG-coated NPs appeared more stable in serum compared to uncoated NPs, but the reduction in total protein adsorbed was most significant for branched PEG coated NP. All PEGylated NPs had similar cellular uptake in HEK-293T and A549 cells. Interestingly, branched-PEG coated NPs had the largest diffusion coefficient and moved most rapidly through Matrigel. However in CF mucus, linear 2 and 5 kDa PEG coated NPs had the largest fraction of rapidly diffusing particles while branched PEG coated NPs had less hindered mobility compared to linear 10 kDa PEG coated NPs.

Conclusion—Branched PEGylation may have the potential to increase NP efficiency in reaching target cells based on an apparent increase in diffusion through an ECM model while maintaining NP stability and uptake in target cells comparable to their linear PEG counterparts.

Keywords—Nanomedicine, PEGylation, Extracellular matrix.

Address correspondence to Gregg A. Duncan, Fischell Department of Bioengineering, University of Maryland, College Park, MD 20742, USA. Electronic mail: gaduncan@umd.edu

INTRODUCTION

Nanoparticle (NP) drug delivery systems have proven useful in enhancing the efficacy of small molecule and nucleic acid-based drugs. Encapsulation of therapeutics in NPs increases the bioavailability of drugs with poor solubility, prevents their degradation, and enables their entry into target cells.[4,19,24] However, from their time of entry into the bloodstream until they reach their target, NPs encounter several obstacles that can impede the efficiency of these systems. Some of these obstacles include clearance by the mononuclear phagocyte system (MPS) and extracellular barriers such as the extracellular matrix (ECM) and mucus.[8,14] These biological barriers can significantly reduce NP delivery efficiency leading to both increased costs and side effects of the intended therapies due to the necessity of high doses.

Upon entry into the bloodstream, NPs undergo opsonization which is a process where antibodies, complement components, and other proteins adsorb onto the surface of NPs, forming a protein corona.[2,32] This process enables recognition of the NPs by phagocytes that are part of the MPS which will then rapidly clear the NPs from the bloodstream. The degree of opsonization, and therefore clearance time, is heavily influenced by surface characteristics of NPs such as charge and hydrophobicity.[2] Even if NPs are designed to effectively delay clearance time by the MPS, the ability of NPs to reach target cells is further obstructed by extracellular barriers they may encounter. An important extracellular barrier is the ECM, a structural and protective matrix composed of proteoglycans, fibronectin, elastin, collagens, laminins, and other glycoproteins[9,24]. Mucus primarily consists of mucin glycoproteins that form a hydrogel matrix creating a physical barrier to drug delivery vehicles that are locally administered to tissues such as the eyes,

lung, and female reproductive tract.[30] Electrostatic interactions and steric hindrance can prevent NPs from successfully crossing through the ECM and mucus layer due to the charged domains, hydrophobic domains, and/or pore size of the matrix.[1,31,33]

ECM remodeling is a common feature of many diseases which can further impede NP transport.[11,40] For example, increased ECM deposition is a hallmark of desmoplastic cancers leading to changes in ECM thickness and porosity.[40] To address this, pre-administration of pharmacological agents to reduce ECM production within the tumor microenvironment has been shown to improve the distribution of nanomedicine in pancreatic cancer models.[12,41] In addition, individuals with asthma may exhibit thickening of ECM within the lung parenchyma and reticular basement membrane in the airway wall which could similarly limit the distribution of NPs to target cells.[11,34] In the airways, mucus poses a significant barrier to drug delivery in lung diseases such as CF lung disease and asthma. Studies have shown that mucus from CF patients contains higher concentrations of disulfide bonds and DNA from lysed immune cells, which both lead to a higher mucus elasticity and a reduction in particle diffusion.[6,39] Mucus samples from asthma patients have exhibited changes to their biomolecular composition and increased elastic and viscous moduli compared to healthy mucus which will likely impair NP diffusion.[10,30]

The surface modification of NPs with polyethylene glycol (PEG) is a commonly used method to address these concerns. PEG is a biocompatible, hydrophilic, net-neutrally charged polymer that, when conjugated to the surface of NPs, confers stealth properties to NPs by shielding the NP core from adhesion to biomolecules which can substantially improve their stability in the bloodstream.[32] Several studies have shown that NPs with high-density PEG coatings avoid clearance via MPS and can successfully navigate through extracellular barriers.[16,32] However, one disadvantage of this approach is the reduction of cellular uptake for PEGylated NPs.[32] As another means to address this, branched polymer coatings, including branched PEGylation, have been the subject of several studies showing enhanced circulation time and decreased immune cell interactions when coated on carbon nanotubes and polymeric NPs.[22,42] It is likely that the increased NP circulation time can be attributed to further reduction in protein binding due to the additional steric hindrance from branched polymer architecture.[42] However, it is not clear how the architecture of PEG coatings may affect the stability and bioactivity of NP drug delivery systems. To the best of our knowledge, studies into the role of polymer architecture in NP penetration through ECM and mucus barriers to delivery have not been previously reported.

Motivated by this prior work, we investigate whether combining both high-density PEGylation and polymer branching can improve upon these advantages. To do this, we compare high-density 4-arm branched PEG NPs with linear PEG NPs of varying molecular weights. NP stability in serum is assessed to determine the shielding capabilities of the PEG coatings. The cellular uptake of the NPs is also evaluated to determine if branching negatively or positively influences PEGylated NP internalization. Finally, we assess NP diffusion through Matrigel, an ECM model, and sputum (mucus) collected from CF patients to understand how their properties might influence their distribution through target tissues.

MATERIALS AND METHODS

Nanoparticle Preparation

Polyethylene glycol (PEG) (Creative PEGWorks; JenKem Technologies) was coated on 100 nm fluorescent carboxylate-modified polystyrene (PS-COOH) nanoparticles (Thermo Scientific) via a carboxyl-amine linkage as described in previous work.[20] NPs were coated with either 2 kDa, 5 kDa, or 10 kDa linear methoxy PEG-amine (JenKem Technologies) or with 10 kDa 4-arm PEG with 3 arms hydroxyl-terminated and 1 arm amine-terminated (JenKem Technologies). Particle size and zeta potential were measured in 10 mM NaCl at a concentration of 0.002% at pH 7 using a Nanobrook Omni dynamic light scattering (DLS) instrument (Brookhaven Instruments). Replicate measurements for size and zeta potential were taken for three different batches of NPs.

Determination of PEG Coating Density

The grafting density of PEG molecules onto the NPs was determined using a 1-pyrenyldiazomethane (PDAM; Thermo Scientific) assay as previously described.[37] Briefly, 1 μL of PEG-coated (PS-PEG) NPs was added to 20 μL of a 15 mg/mL Pluronic F127 (Sigma Aldrich) solution in a black half area 96-well plate. 10 μL of a saturated 0.3 mg/mL PDAM solution in methanol was added to each well. Immediately after, the PDAM and NP fluorescent intensities were measured at 340/375 nm and 580/605 nm, respectively. The PDAM fluorescence for PS-PEG NP samples was compared to a standard curve of unconjugated PS-COOH NPs to determine the concentration of the residual carboxylic groups ($C_{\text{PS-PEG}}$). The density of the PEG groups conjugated to the NPs was then cal-

culated as % PEGylation = $(C_{PS\text{-}COOH} - C_{PS\text{-}PEG})/C_{PS\text{-}COOH} \times 100\%$, where $C_{PS\text{-}COOH}$ is the density of carboxyl groups on unmodified NPs as calculated based on information provided by the manufacturer. The conformational regime for the PEG corona was determined by calculating the ratio of the Flory radius (R_F) to the distance between the grafted PEG chains (D).[38] For linear PEG, R_F was calculated as $R_F = \alpha n^{3/5}$ where α is the size of the monomer (0.35 nm for PEG) and N is the number of monomers in the polymer chain.[38] R_F for branched PEG was calculated using a scaling factor (g) for the ratio of the radius of the branched polymer (R_B) to the radius of the linear polymer of equal molecular weight (R_L) which was obtained as $g = \left(\frac{R_B}{R_L}\right)^2 f^{-4/5}$ where f is the number of branches of the polymer ($f = 4$ for PEG-B10).[5] The distance between PEG chains was calculated as $D = 2\sqrt{\frac{A}{\pi}}$ where A is the area occupied by a PEG chain calculated as the inverse of the PEG density.[38] PEG density was determined for 3 separately prepared batches of NPs.

Nanoparticle Cell Uptake

Human embryonic kidney 293T (HEK-293T) cells were seeded on plastic at ~ 3000 cells/cm^2 in high glucose Dulbecco's Modified Eagle Medium (DMEM) and incubated at 37 °C and 5% CO_2. A549 human lung adenocarcinoma cells were seeded on plastic at ~ 3000 cells/cm^2 in Ham's F12K Medium and incubated at 37ºC and 5% CO_2. Cells were passaged upon reaching 70–80% confluency at which time cells were dissociated from the plate using 0.05% trypsin ethylenediaminetetraacetic acid (EDTA) for 2–5 min at 37 °C. To quantify NP uptake in HEK-293T cells, cells were seeded in 24-well plates at 50,000-cells/cm^2 and allowed to adhere to the plate surface overnight. The medium in each well was then replaced with 1 mL of DMEM containing NPs (~ 4×10^{10} particles). The dose of NPs was determined based on fluorescence intensity. A standard curve based on the fluorescence of serially diluted PS-COOH NPs of known concentration was used to calculate the concentration of PS-PEG NPs. The cells were then incubated with the NPs for 2 h after which the media was removed, and the cells were washed with phosphate-buffered saline (PBS) 3 times to remove excess NPs. The cells were dissociated from the wells using 0.05% trypsin EDTA, collected via centrifugation, and then suspended in 0.1% Triton X-100 to lyse the cells. A Spark Multimode microplate reader (Tecan) was used to measure the fluorescence intensity of the samples at an excitation wavelength at 580 nm and emission wavelength at 605 nm. The amount of cell protein content in each well was determined using a BCA assay (Thermo Scientific) according to the manufacturer's protocol. The standard curve was obtained using bovine serum albumin in 0.1% Triton-X 100 (Sigma Aldrich). The cellular uptake efficiency was then calculated as the amount of NPs per μg of cell protein,[3] and each of these experiments were performed in triplicate. To estimate the amount of uptake due to adhesion of the NPs to the cell membrane, the cell uptake experiments were repeated with a 2-h incubation at 4 °C. The percent uptake due to NP adhesion was calculated as the ratio of measured uptake at 4 °C due to non-specific adsorption to measured cellular uptake at 37 °C. To visualize the cell uptake, cells were seeded on plastic coverslips in 6-well plates and incubated with NPs as described above. After removal of the medium, the cell nucleus was stained by washing the cells once with a 1 μg/mL DAPI-methanol working solution and then incubating the cells in the solution for 15 min. The solution was then removed, and the cells were washed once with methanol. The coverslip was then inverted onto a microscope slide using PBS as a mounting medium.

Nanoparticle Stability Studies

The stability of PS-COOH and PS-PEG NPs conjugated with different linear and branched PEG types was assessed in fetal bovine serum (FBS). The NPs were sonicated and then added to FBS at a concentration of 0.01%. Upon addition of the NPs to the FBS, the size of the particles was measured using DLS. The NPs were then incubated at 37 °C and size measurements were taken at various timepoints over 24 h. To measure the amount of protein adsorbed onto the surface of the NPs, NPs were incubated in FBS at 37 °C for 24 h. NPs were then centrifuged at 21,000×g for 30 min after which the supernatant was removed and replaced with PBS. The NPs were washed two more times, and a BCA assay was used to determine the protein content for the final resuspended NPs. The final concentration of NPs was also determined by reading the fluorescence compared to a NP standard curve using a microplate reader. These studies were performed in triplicate for each NP tested.

Fluorescent Video Microscopy and Multiple Particle Tracking (MPT) Analysis

The diffusion of NPs in Matrigel and sputum collected from patients with CF was evaluated as described in our previous work.[13] Briefly, 25 μL of Matrigel (Corning) was added to a microscopy chamber and allowed to gel at 37 °C for 30 min. After gelation, 1 μL of 0.002% w/v NPs were added to the Matrigel and covered with a coverslip. The gels were

then allowed to equilibrate at 37 °C for 30 min prior to imaging. The same process was used for the mucus samples except NPs were added to the gels immediately after the samples were added to the microscopy chambers. The diffusion of NPs was imaged in real-time using a Zeiss 800 LSM microscope with a 63x water-immersion objective and Zeiss Axiocam 702 camera at a frame rate of 33.33 Hz for 10 seconds. NP trajectories and diffusion rate were determined using a MATLAB-based image analysis software to track NP position over time. The time-averaged mean squared displacement (MSD; $\langle \Delta r^2(\tau) \rangle$) as a function of lag time, τ, was calculated from these trajectories as $\langle \Delta r^2(\tau) \rangle = \langle [x(t+\tau) - x(t)]^2 + [y(t+\tau) - y(t)]^2 \rangle$. A representative measure of the diffusion rate was taken as the logarithm (base 10) of the MSD at a time scale of $\tau = 1$ s ($\log_{10}[\mathrm{MSD}_{1\ s}]$). Matrigel experiments were performed in triplicate for each particle type and videos of the NPs were taken in several (≥3) distinct regions of the gel. Mucus from three different CF patients were used for individual sample replicate, and videos were taken in multiple regions for each gel.

CF Sputum Sample Collection

CF sputum samples from patients at the adult CF clinic at Johns Hopkins ($n = 3$) were collected after receiving written informed consent and approval from the Johns Hopkins Institutional Review Board (study NA_00046768). Sputum samples were stored at –80ºC and thawed on ice prior to MPT experiments.

Statistical Analysis

Statistical analysis and graphing of the data were performed using GraphPad Prism 9 (GraphPad Software). A one-way analysis of variance (ANOVA) with a Tukey or Dunnet *post hoc* correction was performed for analysis between groups. For groups with non-Gaussian distributions, Kruskal-Wallis with Dunn's correction was used. Bar graphs show mean and standard deviation and box and whiskers plots show median value and 5th percentile up to 95th percentile. Statistical significance was assessed at $p < 0.05$.

RESULTS

Formulation of High-Density Branched PEG Nanoparticles

To determine the possible combined effects of high density PEGylation and PEG branching on the stability, cellular uptake, and diffusion of NPs through extracellular barriers, we coated NPs with either 10 kDa branched 4-arm PEG (PEG-B10), 10 kDa linear PEG (PEG-L10), 5 kDa linear PEG (PEG-L5), or 2 kDa linear PEG (PEG-L2). EDC-NHS chemistry was used to obtain a high density of PEG molecules conjugated to the NPs. We then measured their size and zeta potential to compare branched and linear PEG-coated NPs. We hypothesized that the PEG-B10 particles would have similar size and surface charge to the PEG-L5 particles due to the attachment of a single 2.5 kDa PEG arm to the surface with the remaining 2.5 kDa arms forming the outer PEG corona (Fig. 1a). As expected, we found NP size increased when grafted with higher molecular weight linear PEG (Fig. 1b). The size of NPs coated with branched 4-arm PEG fell between that of PEG-L10 and PEG-L5 NPs. The surface charge of all PEGylated NPs fell within a near-neutral range (±5 mV) with PEG-B10 particles and PEG-L5 particles registering surface charges of ~ 0 mV (Fig. 1c).

We next characterized the PEGylation density of the NPs to ensure that we were able to formulate the linear and branched PEGylated NPs within the dense brush regime. To do this, we measured the number of carboxyl-functional groups on NPs remaining after PEGylation to determine the number of PEG molecules per surface area of the NPs. No significant difference in PEGylation density was noted between any NP types (Figs. 1d and 1e). To determine the conformational regime of the different PEG coatings, we calculated the ratio of the Flory radius (R_F) to the distance between the PEG molecules (D). All PEGylated NPs tested were well within the dense brush regime, as indicated by an $R_F/D > 2.8$, where we predict a transition from a globular coil to extended brush conformation of PEG within the layer due to crowding on the NP surface.[38] R_F/D also increased significantly as a function of molecular weight for the linear PEG coatings (Fig. 1f). It is worth noting that R_f for PEG-B10 was approximated using scaling relations for branched star polymers.[5] As a result of its more compact structure, PEG brush density for NPs coated with PEG-B10 is predicted to be most similar to that of densely coated PEG-L5 NPs.

Nanoparticle Stability in Serum

Previous studies using branched polymer coatings on NPs observed an increase in NP stability and circulation time *in vivo*.[22,42] We investigated whether these same advantages might be noted for NPs with branched, high density PEG coatings by assessing the stability of the NPs in FBS over a 24-h period. The stability was assessed by measuring NP size over time using DLS (Fig. 2a). Overall size change was expressed as the difference between the NP size at 24 h and the

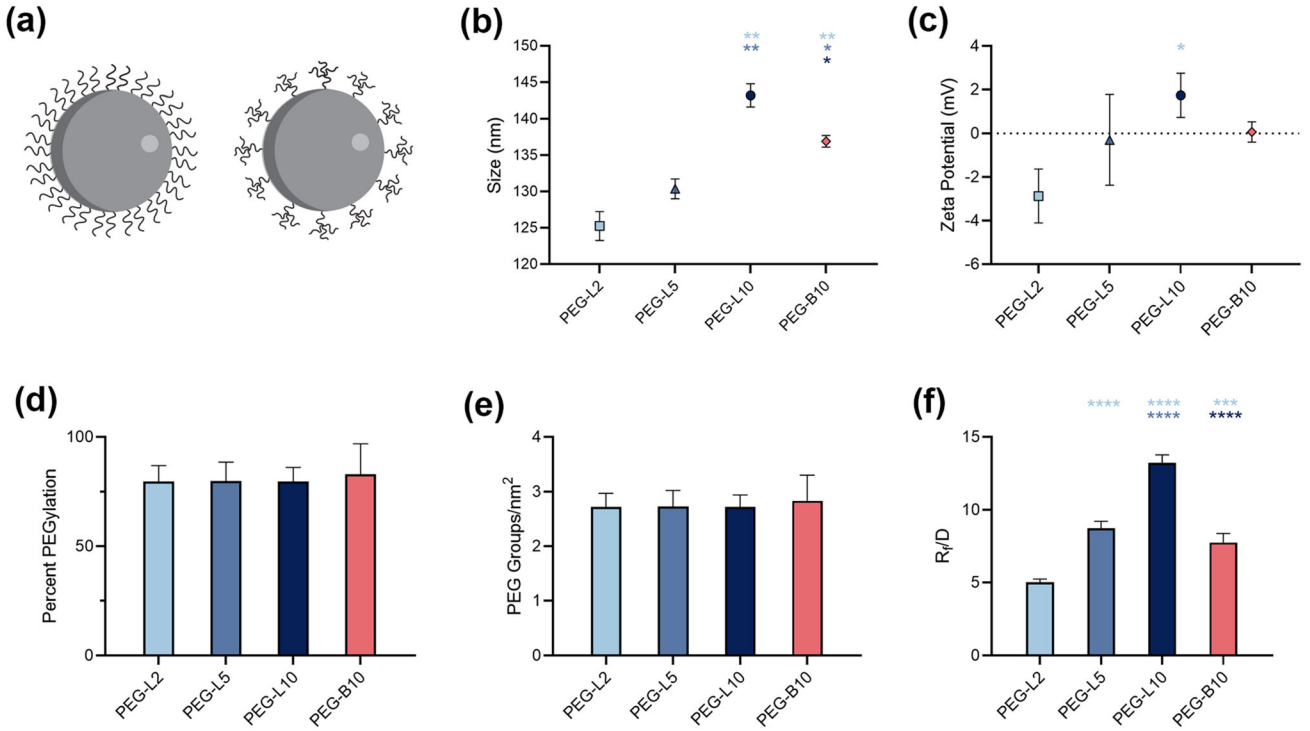

FIGURE 1. Physicochemical characterization of PEGylated NP. (a) Schematic of NP coated with linear (left) or branched (right) PEG. (b) Size (diameter) of NPs conjugated with linear 2 kDa (PEG-L2), 5 kDa (PEG-L5), 10 kDa (PEG-L10) and branched 10 kDA PEG (PEG-B10). (c) Zeta potential of NPs with PEG coatings. (d, e) PEGylation density for each NP type characterized as (*D*) the percent of carboxylic acid groups conjugated to PEG and (e) the number of PEG per unit surface area of the NPs. (f) Ratio of the Flory radius (R_F) to the distance between PEG chains on NP (*D*) where the dense brush regime is defined as $R_f/D > 2.8$. *$p < 0.05$ by one-way ANOVA, **$p < 0.005$ by one-way ANOVA, ***$p < 0.001$ by one-way ANOVA, ****$p < 0.0001$ by one-way ANOVA. The comparison group is indicated by the color of the asterisk. Data represents the average of 3 replicates from separately prepared batches of PEGylated NPs.

initial measurement (Fig. 2b). There was no significant difference in the overall size change for the different types of PEGylated NPs. PEG-coated NPs had a relatively small change in size when compared to NPs without any PEG coating (Fig. 2b). Non-PEGylated NPs also had visible flocculation after 20 h for one of the replicates. These larger aggregates quickly settle and are unlikely to be detected in our measurements. With the aim of determining whether stability was directly correlated to protein adsorption, we estimated the amount of protein adhered to NP surfaces (Fig. 2c). Of note, only PEG-B10 NPs exhibited a statistical difference in protein adsorption compared to unPEGylated NPs.

Nanoparticle Cellular Uptake In Vitro

We next investigated whether branched polymer coatings influenced cellular uptake as compared to NPs formulated with dense linear PEG coatings. We hypothesized PEG branching may reduce cellular uptake due to its resistance to adhesion to biomolecules which in turn would reduce its association to the cell surface and internalization. We evaluated the uptake of our NPs in two different cell lines, HEK-293T and A549 cells, as it has been reported that cellular uptake of PEGylated NP may vary dependent on the type of cells tested.[29] Overall, we found a higher uptake of NPs in the A549 cell line compared to the HEK-293T cell line for all conditions. In the HEK-293T cell line, the PEG-L5, PEG-L10 and PEG-B10 NPs had a higher average cell uptake compared to the unPEGylated NPs (Figs. 3a, 3b). However, these differences were not statistically significant. The uptake of the NPs was also verified qualitatively via cell staining and imaging. We observed that the PEG-B10 NPs were associated with the HEK-293T cells, and few to no NPs were observed outside of the cell regions (Fig. 3c). Unlike in the HEK-293T cell line, the non-PEGylated and PEGylated particles had a similar uptake compared to the rest of the coated NPs (Fig. 3d and 3e). There was no statistical difference between any of the conditions for uptake in the A549 cell line, and no discernable trend was noted. Association and/or uptake of PEG-B10 NP was also apparent based on fluorescent micrographs in A549 cells (Fig. 3f). To determine whether uptake

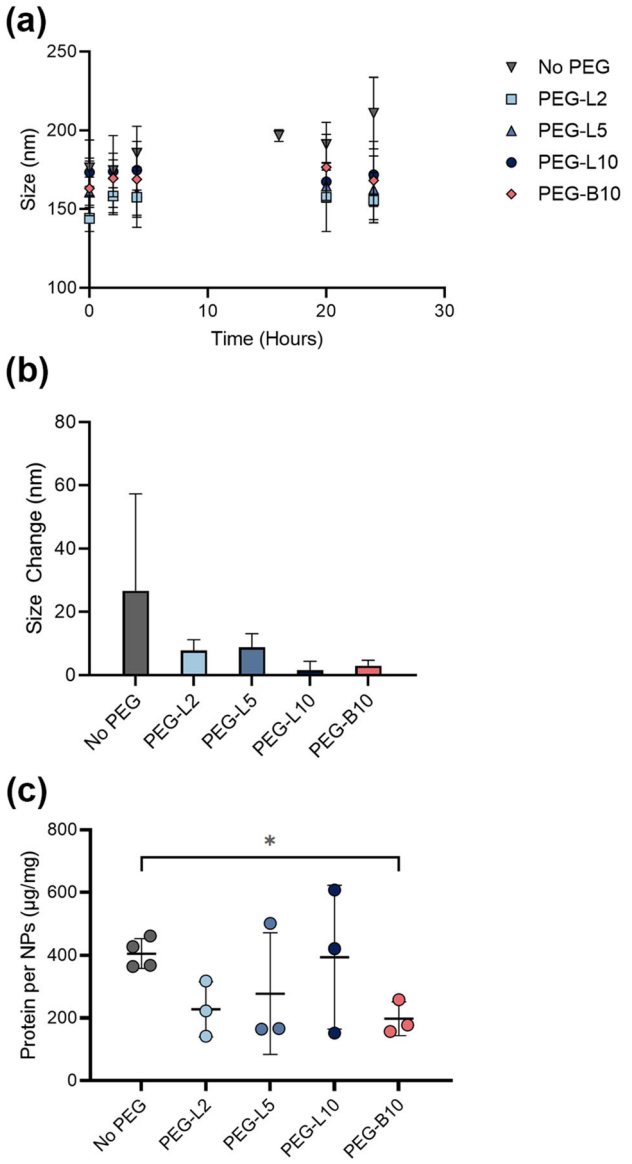

FIGURE 2. Stability of nanoparticles in fetal bovine serum (FBS) over a 24-h period. (a) Size of unPEGylated NP (No PEG) and NP conjugated with 2 kDa (PEG-L2), 5 kDa (PEG-L5), 10 kDa (PEG-L10) and branched 10 kDa PEG (PEG-B10) in FBS over a 24-h period. (b) Overall change in size of NPs in FBS over a 24-h period. (c) Protein adsorption onto NP surface over a 24-h period. *$p < 0.05$ by one-way ANOVA with Dunnet Correction. Replicates ($n = 3$) were NPs incubated in serum 3 separate times.

measurements were appreciably affected by NP adsorption to cell membranes, we measured the uptake of NPs after a cold (4 °C) incubation period (Fig. 3g). We found that less than 10% of the uptake was due to membrane adhesion for all types of NPs (Fig. 3h). There was no statistical difference between membrane adhesion for any NP types. However, non-PEGylated NPs had the highest percentage of membrane adsorbed NP.

Diffusion of Nanoparticles in an ECM Model

Increased PEGylation density is known to increase NP diffusion through extracellular barriers such as the ECM and mucus.[16,32] We hypothesized that a densely PEGylated NP with a branched PEG coating would have enhanced diffusion capabilities in comparison to NPs with a similarly dense linear PEG coating. We reasoned this would result from the effective increase in PEG arms per unit NP surface area, enhancing the stealth properties of the NPs. We chose Matrigel, which is a mouse basement membrane matrix, as an *in vitro* ECM model to investigate whether PEG branching had any effect on NP diffusion properties. We measured and analyzed the trajectories of the different NP types in the Matrigel model which were used to calculate the MSD and effective diffusion coefficients (D_{eff}) of the different NPs (Fig. 4). Qualitatively, the non-PEGylated NPs seemed completely motionless within the matrix while there was more noticeable mobility for the linear PEG NPs and significant diffusion was apparent for the PEG-B10 NPs (Fig. 4a). The MSD and D_{eff} values were significantly different between all types of NPs (Figs. 4b and 4c). Overall, PEG-B10 NPs had the highest D_{eff} values while the non-PEGylated NPs had the lowest (Fig. 4d). Among the linear PEG NPs, the PEG-L5 NPs had significantly higher D_{eff} values than the PEG-L2 and PEG-L10 NPs, and the PEG-L10 particles had a higher D_{eff} than the PEG-L2 NPs. Considering only motion in 1 direction (e.g. vertical or z–direction) and assuming standard (Brownian) diffusion, we calculated the time it would take for uncoated and PEGylated NPs to cross 1 μm-thick basement membrane based on our MPT results. Comparing across cases, PEG-B10 NPs are predicted to cross the same thickness of ECM >30 times faster than all other NPs tested (Fig. 4e).

Diffusion of Nanoparticles in Mucus

As noted, coating NPs in PEG has been shown to increase NP mobility in mucus, but higher MW PEG can become entangled with the mucus mesh, impeding benefits of the coating.[35] However, previous studies have shown that densely coating NPs in PEG can increase their mobility in mucus even with PEG of higher MW.[16] Based on our studies in Matrigel, we hypothesized that NPs with a dense branched PEG coating would have improved diffusion profiles in mucus compared to NPs coated with linear PEG of a similar coating density. To test this, we measured and analyzed the trajectories of the different NP types in mucus samples collected from three individuals with CF lung disease (Fig. 5). Qualitatively, the non-PEGylated NPs seemed completely immobile within the gel while

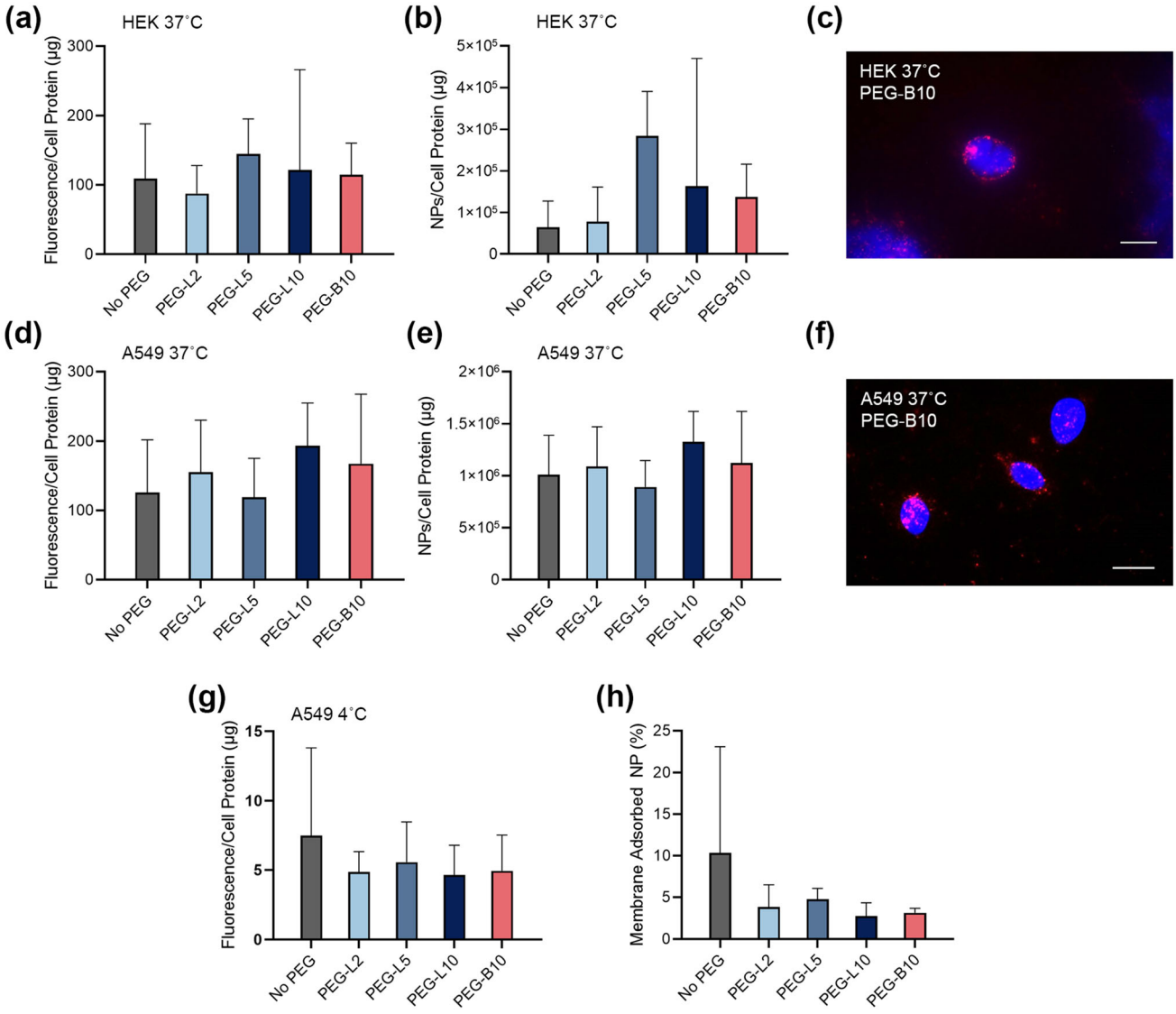

FIGURE 3. ***In vitro*** **cellular uptake of linear and branched PEG coated nanoparticles. NP uptake was evaluated in HEK-293T (a–c) and (d–f) A549 cells. Uptake was quantified based on NP fluorescence and number of NPs per cell protein content in (a, b) HEK-293T and A549 (d, e) cells. Fluorescent micrographs of HEK-293T (c) and A549 (f) cells after a 2-h incubation with NPs where the NPs are visualized in red and the cell nucleus in blue. Scale bar = 20 μm. (g) NP uptake in A549 cells at 4 °C representing NPs adsorbed to the cell surface. (h) Percent of total uptaken NPs adsorbed to cell membrane surface. n = 3 for all uptake experiments.**

there was more noticeable mobility for the PEGylated NPs and significant diffusion was apparent for the PEG-L2 and PEG-L5 NPs (Fig. 5a). To quantitatively compare PEG types, we looked at the distribution of MSD and the proportion of particles that rapidly penetrated mucus defined as those with MSD ≥ 1 μm^2 or $\log_{10}$MSD ≥ 0 at 1 second. Considering motion only in the vertical direction, we would predict this population would transport through a mucus layer of physiological thickness, ranging from 10 to 50 μm, in under an hour and avoid removal from the lung via mucociliary clearance.[26,30] The vast majority (~ 99%) of non-PEGylated NP are predicted to be immobilized by the mucus barrier and cleared from the lung before reaching target cells (Fig. 5b). Comparing across PEGylated NPs, PEG-L2 and PEG-L5 NPs were found to have the largest fraction of NPs, 49% and 40%, respectively, that rapidly penetrate CF mucus (Figs. 5c and 5d). There was a larger amount of variance in individual particle diffusion for PEG-L10 (Fig. 5e) and PEG-B10 NPs (Fig. 5f). However, PEG-B10 NPs had a greater fraction (~ 32%) of NPs that rapidly penetrate the mucus barrier as compared to PEG-L10 NP (23%).

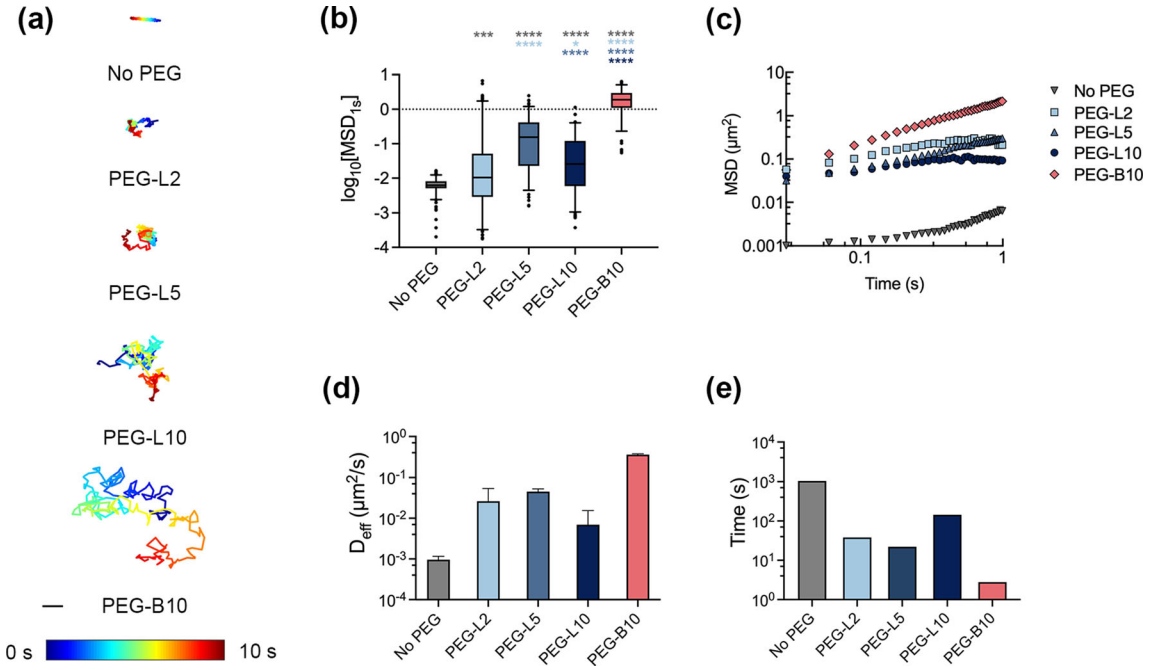

FIGURE 4. Diffusion of nanoparticles coated with linear and branched PEG through a Matrigel ECM model. (a) Representative trajectories of unPEGylated and PEGylated NPs in Matrigel. Traces show 10 seconds of motion with a color scale to indicate time. The scale bar represents 1 μm. (b) Calculated log based 10 of MSD at $\tau = 1$ s ($\log_{10}[MSD_{1s}]$) of NPs in Matrigel. (c) Average MSD over time for NPs. (d) Measured diffusion coefficients (D_{eff}) for different NP types. (e) Estimated time to cross 1 μm thick basal lamina as calculated from D_{eff}. ***$p < 0.001$ by Kruskal-Wallis with Dunn's correction, ****$p < 0.0001$ by Kruskal-Wallis with Dunn's correction. The comparison group is indicated by the color of the asterisk. At least three videos in different regions of the gel were acquired and analyzed in each experiment. An average of > 160 particles were tracked per sample tested.

DISCUSSION

In this study, we designed NPs with dense branched PEG coatings and explored their potential utility for drug delivery applications. We demonstrated NPs can be formulated with 4-arm branched PEG coatings with a similar PEG density when compared to linear PEG coatings of various molecular weights. To accomplish this, we used a 4-arm PEG star polymer with three non-reactive hydroxyl terminated arms and one arm functionalized with a reactive amine group. This means for every functionalized arm conjugated to the NP surface, an additional three nonfunctionalized arms were protruding from the polymer core extending out to form a branched PEG corona. While bulkier, we found monofunctional 4-arm PEG could be conjugated at a high density like that obtained using linear PEG chains. Furthermore, we expect that branched PEG coverage on the nanoparticle surface for the PEG-B10 NPs are underestimated based on our brush regime (R_f/D) calculations. In effect, we expect that branching would lead to higher PEG surface coverages due to the higher number of chains per PEG molecule. However, additional theoretical models and/or direct measurements of PEG density profiles are necessary to fully assess the impact of branching on the PEG corona. Previous studies have established a critical R_f/D for linear PEG-coated NP that are predictive of diffusion through mucus.[26,36] However, such guidelines do not exist for branched PEG and the current guidelines would need to be revised based on our current data. In future work, it will be important to evaluate the performance of branched PEG-coated NPs with varying surface density to establish these criteria. Furthermore, we have yet to explore if the extent of branching (e.g. 2-arm vs. 4-arm vs. 6-arm) has any functional significance on NP PEGylation.

When examining the effects of the PEG corona on NP stability, we measured the size change of the nanoparticles over a 24-h period as a marker of serum protein adsorption and particle aggregation. We found that there was no significant size change for linear or branched PEGylated NPs. The larger average size of non-PEGylated NPs would indicate a greater extent of serum protein adsorption on non-PEGylated as compared PEGylated NPs. We did not find a significantly larger size change indicative of particle instability and aggregation. However, we note that a set of non-PEGylated NPs exhibited visible flocculation after 20 h, which was not seen in any PEGylated NP types. Prencipe *et al.* showed that PEGylated branched polymers yielded NPs with increased stability in serum as well as

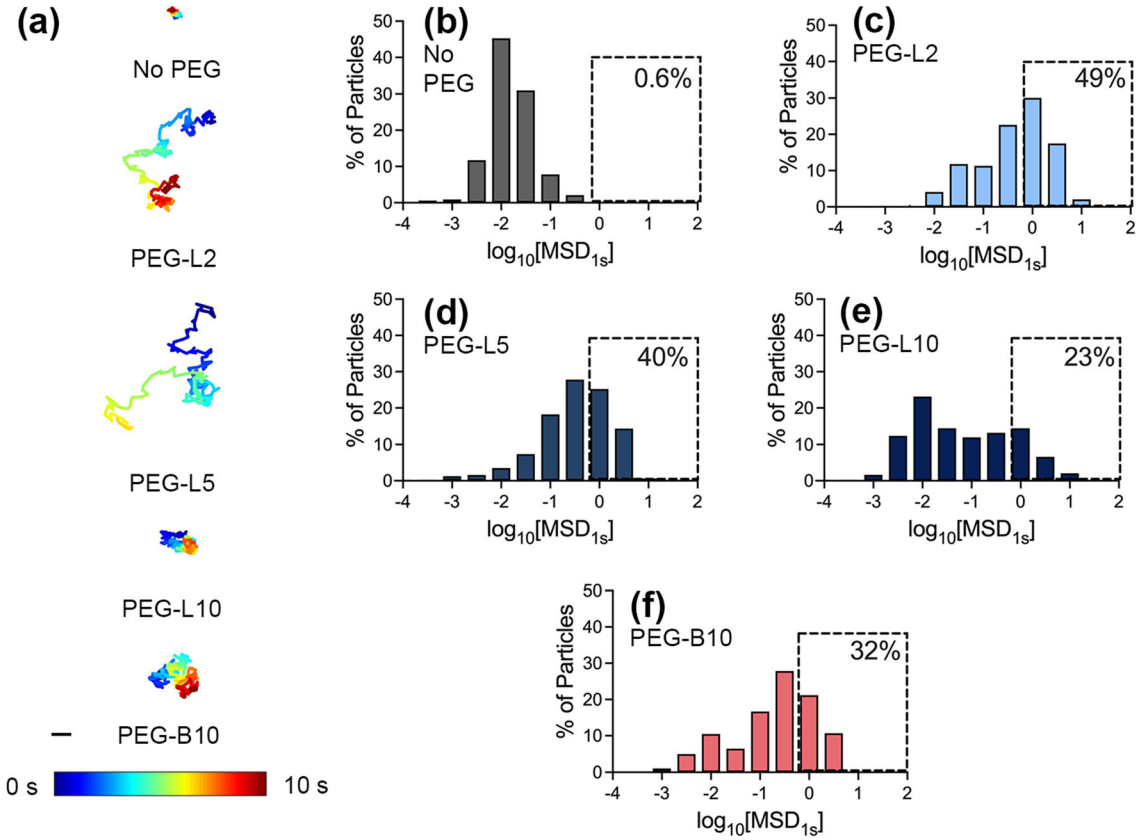

FIGURE 5. Diffusion of nanoparticles coated with linear and branched PEG through mucus from individuals with cystic fibrosis (CF). (a) Representative trajectories of unPEGylated NP (No PEG) and linear 2 kDa (PEG-L2), linear 5 kDa (PEG-L5), linear 10 kDa (PEG-L10), branched 10 kDa (PEG-B10) PEGylated NPs in CF mucus. Traces show 10 seconds of motion with a color scale to indicate time. The scale bar represents 1 μm. Distribution of log based 10 of MSD at τ = 1 s ($\log_{10}[MSD_{1s}]$) for (b) UnPEGylated NP, (c) PEG-L2 NP, (d) PEG-L5 NP, (e) PEG-L10 NP, (f) PEG-B10 NP. Data represent the average of three sputum samples, with an average of > 400 particles tracked per sample tested. Percentage of particles that moved rapidly, defined as $\log_{10}$MSD ≥ 0 at a time scale of 1 s, is shown for each particle type (dashed boxes).

a higher blood circulation half-life.[22] This led us to hypothesize that the 4-arm branched PEG nanoparticles would exhibit reduced protein adsorption and greater stability compared to the other conditions. While the results did not entirely fit our hypothesis, it is worth noting that PEG-L10 and PEG-B10 NPs exhibited minimal size change (< 3 nm) over the 24-h period. PEG-L2 and PEG-L5 NPs exhibited detectable changes (> 7 nm) in size over 24 h indicative of protein adsorption.

To confirm our hypothesis that protein adhesion was causing the increase in NP size measurements, we also measured the adsorption of proteins onto NPs. We found a higher amount of protein for the unPEGylated NPs compared to the PEGylated NPs except with respect to the PEG-L10 NPs. However, differences were only significant between the unPEGylated and PEG-B10 NPs. Our measurements of protein adsorption indicate a significantly lower adsorption for PEG-B10 NPs compared to unPEGylated NPs, fitting our initial hypothesis. Although PEG-L10 NPs exhibited minimal size change over 24 h, they exhibited comparable protein adsorption to unPEGylated NPs. This is counter-intuitive as it would be expected longer PEG chains would significantly limit protein adsorption.[28] This may suggest differences in protein corona conformation (e.g. hard, irreversible vs. soft, exchangeable protein coronas[21]) for the PEG-L10 NPs, but further analyses is required to determine if this is the case. It is possible that branched polymer coatings, independent of surface density, are sufficient to prevent protein adhesion and serum opsonization, which may in part explain the long (~ 22 h) circulation half-life of branched PEG coated carbon nanotubes reported in previous work.[22] However, further work is required to compare serum stability of branched PEG with varied surface density.

We assessed the cellular uptake of NPs using two different cell lines. Our non-PEGylated control were net-negatively charged, carboxylate (COO−) modified PS NP used throughout our studies to generate densely PEGylated NP. Cells generally preferentially uptake

positively charged NPs since the cell membrane is negatively charged.[25] Furthermore, negatively charged NPs are generally uptaken through caveolae-mediated endocytosis whereas positively charged NPs are preferentially uptaken through clathrin-mediated endocytosis.[17] Consequently, differences in the uptake pathway due to the negative charge of the non-PEGylated NPs may explain the comparable uptake to densely PEGylated NPs.[17] It has also been reported that PEGylation can differentially impact cellular uptake and that the degree of uptake can also vary between cell types. Therefore, we studied uptake in two different cell lines that were previously noted to have different trends in the extent of cellular uptake and influence of PEGylation on uptake.[7,15,18,23] The uptake of the non-PEGylated NPs was lower than all the PEGylated NPs except for PEG-L2 in the HEK-293T cell line, however, the differences were not statistically significant. Nonetheless, our studies would indicate branched PEGylation does not significantly alter the uptake of PEGylated NPs as compared to NPs with linear PEG coatings with similar dimensions.

We found that PEGylation resulted in greater diffusivity of NPs through an ECM model (Matrigel) as evidenced by a greater MSD and D_{eff}, which is consistent with several previously reported studies.[27,32,37] Interestingly, the branched PEG NPs resulted in a significantly higher rate of diffusion when compared to all other PEG types. In addition, we measured the diffusion of PEGylated NPs in sputum collected from individuals with CF lung disease. Given inhaled nanomedicine approaches have been explored for CF, we felt this would provide initial evidence to support the use of branched PEGylation for these applications. Prior work has shown increasing molecular weight of linear PEG reduces their ability to penetrate CF sputum.[35] However, we found PEG-B10 NPs had greater mobility within mucus layer compared to PEG-L10 NPs. This may be the result of restricted mobility of PEG chains in the branched conformation as previous work has shown NPs with ultra-high density, high MW (> 10 kDa) PEG coatings retain mucus-penetrating capabilities.[16]

For comparison to prior work on PEGylated NP diffusion through mucus, low molecular weight PEG coatings were shown to reduce interactions of the nanoparticle with the matrix without significant entanglement, allowing for greater diffusivity.[35] Specifically, Wang *et al.* found that nanoparticles coated with either 2 or 5 kDa PEG did not adhere to the mucus mesh with a slightly higher MSD for the 5 kDa PEG NPs while those coated with 10 kDa PEG had severely limited diffusion due to entanglements with the mucus mesh.[35] However, it has been noted that a sufficiently dense PEG coating can prevent these entanglements even with higher molecular weight PEG.[16] We observed a similar trend in Matrigel with our linear PEG coated NPs where the PEG-L5 particles had the highest MSD presumably due to enhanced shielding compared to the PEG-L2 particles and less entanglements with the matrix compared to the PEG-L10 particles. However, we find the greatest diffusivity for PEG-L2 coated NP in CF sputum which further reduces the possibility of entanglements and hydrogen bonding with the mucus gel network.[35] Based on the apparent enhancement in diffusion through Matrigel for PEG-B10 NP, it is possible that PEG branching further prevents entanglement with the gel since it is already very sterically limited. This may have led to an ideal balance where the PEG-B10 coating is able to block interactions with the ECM while simultaneously preventing entanglements, yielding enhanced mobility. However, the molecular weight of PEG-B10 would allow for a greater extent of mucin-PEG hydrogen bonding leading to reduced NP diffusivity compared to linear PEG of lower molecular weight. Overall, these results suggest that branched PEG coatings could potentially benefit NP drug delivery systems to overcome the ECM barrier that impedes their efficacy which will be explored further in future work. It will also be of future interest to evaluate branched PEG coatings of varied molecular weight (e.g. MW < 10 kDa) to determine if this alters mucus-penetrating properties of PEGylated NP.

CONCLUSIONS

Our results show that branched PEG can be successfully coated onto NPs at a high-density comparable to that of linear PEG-coatings. These high-density branched PEG coatings provided comparable benefits to stability of NPs in serum with linear PEG-coated NPs, suggesting they effectively limit serum protein adsorption. Branched PEG coatings also did not adversely affect NP uptake in two different cell lines. We demonstrated that these high-density branched PEG coatings may significantly increase the diffusion profile of NPs in ECM compared to linear PEG-coated NPs and in mucus compared to linear PEG-coated NPs of the same MW. The findings of this study suggest that high-density branched PEG NPs may be useful in addressing obstacles in drug delivery and present an opportunity to achieve greater accumulation of NPs at the target site.

ACKNOWLEDGMENTS

We thank Dr. Steven Jay and Dr. Margaret Scull at the University of Maryland for generously providing HEK-293T and A549 cells, respectively. We thank Dr. Natalie West, Dr. Jung Soo Suk, and Dr. Justin Hanes at Johns Hopkins University School of Medicine for providing the CF sputum used in our work through their IRB-approved study. We acknowledge the BioWorkshop core facility in the Fischell Department of Bioengineering at the University of Maryland for use of their dynamic light scattering instrument and microplate reader.

FUNDING

This work was supported by the American Lung Association Innovation Award, Burroughs Wellcome Fund Career Award at the Scientific Interface, NSF CAREER Award 2047794, and UMD-NCI Partnership for Integrative Cancer Research.

CONFLICT OF INTEREST

Devorah Cahn and Gregg Duncan declare no conflicts of interest.

HUMAN SUBJECTS RESEARCH ETHICS STATEMENT

Human mucus was collected under an IRB-approved protocol at the Johns Hopkins University of School of Medicine (Study NA_00046768). Spontaneously expectorated sputum samples were collected after receiving written informed consent from all patients included in the study. All patient samples were de-identified and referred to by numerical ID only.

ANIMAL RESEARCH ETHICS STATEMENT

No animal studies were performed in this research.

REFERENCES

[1]Arends, F., R. Baumgärtel, and O. Lieleg. Ion-specific effects modulate the diffusive mobility of colloids in an extracellular matrix gel. *Langmuir*. 29(51):15965–15973, 2013. https://doi.org/10.1021/LA404016Y/SUPPL_FILE/LA404016Y_SI_001.PDF.

[2]Blanco, E., H. Shen, and M. Ferrari. Principles of nanoparticle design for overcoming biological barriers to drug delivery. *Nat Biotechnol*. 33(9):941–951, 2015. https://doi.org/10.1038/nbt.3330.

[3]Chen, J., S. Li, Q. Shen, H. He, and Y. Zhang. Enhanced cellular uptake of folic acid conjugated PLGAPEG nanoparticles loaded with vincristine sulfate in human breast cancer. *Drug Dev. Ind. Pharm*. 37(11):1339–1346, 2011. https://doi.org/10.3109/03639045.2011.575162.

[4]Dai, Q., N. Bertleff-Zieschang, J. A. Braunger, M. Björnmalm, C. Cortez-Jugo, and F. Caruso. Particle targeting in complex biological media. *Adv. Healthc. Mater*. 7(1):1700575, 2018. https://doi.org/10.1002/ADHM.201700575.

[5]Daoud, M., and J. P. Cotton. Star shaped polymers: a model for the conformation and its concentration dependence. *J. Phys. Paris*. 43(3):531–538, 1982. https://doi.org/10.1051/jphys:01982004303053100.

[6]Duncan, G. A., J. Jung, A. Joseph, et al. Microstructural alterations of sputum in cystic fibrosis lung disease. *JCI Insight*. 1(18):88198, 2016. https://doi.org/10.1172/JCI.INSIGHT.88198.

[7]Evensen, L., P. L. Johansen, G. Koster, et al. Zebrafish as a model system for characterization of nanoparticles against cancer. *Nanoscale*. 8(2):862–877, 2015. https://doi.org/10.1039/C5NR07289A.

[8]Finbloom, J. A., F. Sousa, M. M. Stevens, and T. A. Desai. Engineering the drug carrier biointerface to overcome biological barriers to drug delivery. *Adv. Drug Deliv. Rev*. 167:89–108, 2020. https://doi.org/10.1016/J.ADDR.2020.06.007.

[9]Frantz, C., K. M. Stewart, and V. M. Weaver. The extracellular matrix at a glance. *J. Cell Sci*. 123(123):4195–4200, 2010. https://doi.org/10.1242/jcs.023820.

[10]Innes, A. L., S. D. Carrington, D. J. Thornton, et al. Ex vivo sputum analysis reveals impairment of protease-dependent mucus degradation by plasma proteins in acute asthma. *Am. J. Respir. Crit. Care Med*. 180(3):203, 2009. https://doi.org/10.1164/RCCM.200807-1056OC.

[11]James, A. L., P. S. Maxwell, G. Pearce-Pinto, J. G. Elliot, and N. G. Carroll. The relationship of reticular basement membrane thickness to airway wall remodeling in asthma. *Am. J. Respir. Crit. Care Med*. 166(12 Pt 1):1590–1595, 2002. https://doi.org/10.1164/rccm.2108069.

[12]Ji, T., J. Lang, J. Wang, et al. Designing liposomes to suppress extracellular matrix expression to enhance drug penetration and pancreatic tumor therapy. *ACS Nano*. 11(9):8668–8678, 2017. https://doi.org/10.1021/ACSNANO.7B01026/SUPPL_FILE/NN7B01026_SI_001.PDF.

[13]Lee, B. J., Y. Cheema, S. Bader, and G. A. Duncan. Shaping nanoparticle diffusion through biological barriers to drug delivery. *JCIS Open*.4:100025, 2021. https://doi.org/10.1016/J.JCISO.2021.100025.

[14]Lieleg, O., R. M. Baumgärtel, and A. R. Bausch. Selective filtering of particles by the extracellular matrix: an electrostatic bandpass. *Biophys J*. 97(6):1569, 2009. https://doi.org/10.1016/J.BPJ.2009.07.009.

[15]Magno, L. M., D. T. Hinds, P. Duffy, et al. Porous carbon microparticles as vehicles for the intracellular delivery of molecules. *Front. Chem*. 8:925, 2020. https://doi.org/10.3389/FCHEM.2020.576175/BIBTEX.

[16]Maisel, K., M. Reddy, Q. Xu, et al. Nanoparticles coated with high molecular weight PEG penetrate mucus and provide uniform vaginal and colorectal distribution in vivo. *Nanomedicine*. 11(11):1337–1343, 2016. https://doi.org/10.2217/nnm-2016-0047.

[17]Manzanares, D., and V. Ceña. Endocytosis: the nanoparticle and submicron nanocompounds gateway into the cell.

Pharmaceutics. 12(4):371, 2020. https://doi.org/10.3390/PHARMACEUTICS12040371.
[18]Marazioti, A., K. Papadia, M. Kannavou, et al. Cellular vesicles: New insights in engineering methods, interaction with cells and potential for brain targeting. *J. Pharmacol. Exp. Ther*. 370(3):772–785, 2019. https://doi.org/10.1124/JPET.119.257097/-/DC1.
[19]Mitchell, M. J., M. M. Billingsley, R. M. Haley, M. E. Wechsler, N. A. Peppas, and R. Langer. Engineering precision nanoparticles for drug delivery. *Nat. Rev. Drug Discov*. 20(2):101, 2021. https://doi.org/10.1038/S41573-020-0090-8.
[20]Nance, E. A., G. F. Woodworth, K. A. Sailor, et al. A dense poly(ethylene glycol) coating improves penetration of large polymeric nanoparticles within brain tissue. *Sci. Transl. Med*. 4(149):149ra119, 2012. https://doi.org/10.1126/SCITRANSLMED.3003594.
[21]Nel, A. E., L. Mädler, D. Velegol, et al. Understanding biophysicochemical interactions at the nano-bio interface. *Nat. Mater*. 8(7):543–557, 2009. https://doi.org/10.1038/NMAT2442.
[22]Prencipe, G., S. M. Tabakman, K. Welsher, et al. PEG branched polymer for functionalization of nanomaterials with ultralong blood circulation. *J. Am. Chem. Soc*. 131(13):4783–4787, 2009. https://doi.org/10.1021/ja809086q.
[23]Rojnik, M., P. Kocbek, F. Moret, et al. In vitro and in vivo characterization of temoporfin-loaded PEGylated PLGA nanoparticles for use in photodynamic therapy. *Nanomedicine*. 7(5):663–677, 2012. https://doi.org/10.2217/NNM.11.130/ASSET/IMAGES/LARGE/FIGURE9.JPEG.
[24]Rosenblum, D., N. Joshi, W. Tao, J. M. Karp, and D. Peer. Progress and challenges towards targeted delivery of cancer therapeutics. *Nat. Commun*. 2018. https://doi.org/10.1038/s41467-018-03705-y.
[25]Saadat, M., F. Zahednezhad, P. Zakeri-Milani, H. R. Heidari, J. Shahbazi-Mojarrad, and H. Valizadeh. Drug targeting strategies based on charge dependent uptake of nanoparticles into cancer cells. *J. Pharm. Pharm. Sci*. 22(1):191–220, 2019.
[26]Schneider, C. S., Q. Xu, N. J. Boylan, et al. Nanoparticles that do not adhere to mucus provide uniform and long-lasting drug delivery to airways following inhalation. *Sci. Adv*. 2017. https://doi.org/10.1126/sciadv.1601556.
[27]Schuster, B. S., J. S. Suk, G. F. Woodworth, and J. Hanes. Nanoparticle diffusion in respiratory mucus from humans without lung disease. *Biomaterials*. 34(13):3439–3446, 2013. https://doi.org/10.1016/j.biomaterials.2013.01.064.
[28]Shi, L., J. Zhang, M. Zhao, et al. Effects of polyethylene glycol on the surface of nanoparticles for targeted drug delivery. *Nanoscale*. 13(24):10748–10764, 2021. https://doi.org/10.1039/D1NR02065J.
[29]Soenen, S. J., B. B. Manshian, A. M. Abdelmonem, et al. The cellular interactions of PEGylated gold nanoparticles: effect of PEGylation on cellular uptake and cytotoxicity. *Part. Part. Syst. Charact*. 31(7):794–800, 2014. https://doi.org/10.1002/PPSC.201300357.
[30]Song, D., D. Cahn, and G. A. Duncan. Mucin biopolymers and their barrier function at airway surfaces. *Langmuir*. 2020. https://doi.org/10.1021/acs.langmuir.0c02410.
[31]Stylianopoulos, T., M. Z. Poh, N. Insin, et al. Diffusion of particles in the extracellular matrix: the effect of repulsive electrostatic interactions. *Biophys J*. 99(5):1342–1349, 2010. https://doi.org/10.1016/j.bpj.2010.06.016.
[32]Suk, J. S., Q. Xu, N. Kim, J. Hanes, and L. M. Ensign. PEGylation as a strategy for improving nanoparticle-based drug and gene delivery. *Adv. Drug Deliv Rev*. 99:28–51, 2016. https://doi.org/10.1016/j.addr.2015.09.012.
[33]Tomasetti, L., R. Liebl, D. S. Wastl, and M. Breunig. Influence of PEGylation on nanoparticle mobility in different models of the extracellular matrix. *Eur. J. Pharm. Biopharm*. 108:145–155, 2016. https://doi.org/10.1016/j.ejpb.2016.08.007.
[34]Vignola, A. M., J. Kips, and J. Bousquet. Tissue remodeling as a feature of persistent asthma. *J. Allergy Clin. Immunol*. 105(6):1041–1053, 2000. https://doi.org/10.1067/MAI.2000.107195.
[35]Wang, Y. Y., S. K. Lai, J. S. Suk, A. Pace, R. Cone, and J. Hanes. Addressing the PEG mucoadhesivity paradox to engineer nanoparticles that "slip" through the human mucus barrier. *Angew. Chem. Int. Ed*. 47(50):9726–9729, 2008. https://doi.org/10.1002/anie.200803526.
[36]Xu, Q., L. M. Ensign, N. J. Boylan, et al. Impact of surface polyethylene glycol (PEG) density on biodegradable nanoparticle transport in mucus ex vivo and distribution in vivo. *ACS Nano*. 9(9):9217–9227, 2015. https://doi.org/10.1021/acsnano.5b03876.
[37]Yang, Q., S. W. Jones, C. L. Parker, W. C. Zamboni, J. E. Bear, and S. K. Lai. Evading immune cell uptake and clearance requires PEG grafting at densities substantially exceeding the minimum for brush conformation. *Mol. Pharm*. 11(4):1250–1258, 2014. https://doi.org/10.1021/mp400703d.
[38]Yang, Q., and S. K. Lai. Engineering well-characterized PEG-coated nanoparticles for elucidating biological barriers to drug delivery. *Methods Mol. Biol*. 1530:125–137, 2017. https://doi.org/10.1007/978-1-4939-6646-2_8.
[39]Yuan, S., M. Hollinger, M. E. Lachowicz-Scroggins, et al. Oxidation increases mucin polymer cross-links to stiffen airway mucus gels. *Sci. Transl. Med*. 7(276):276ra27, 2015. https://doi.org/10.1126/SCITRANSLMED.3010525.
[40]Zámecník, J., L. Vargová, A. Homola, R. Kodet, and E. Syková. Extracellular matrix glycoproteins and diffusion barriers in human astrocytic tumours. *Neuropathol. Appl. Neurobiol*. 30(4):338–350, 2004. https://doi.org/10.1046/j.0305-1846.2003.00541.x.
[41]Zhang, B., T. Jiang, S. Shen, et al. Cyclopamine disrupts tumor extracellular matrix and improves the distribution and efficacy of nanotherapeutics in pancreatic cancer. *Biomaterials*. 103:12–21, 2016. https://doi.org/10.1016/J.BIOMATERIALS.2016.06.048.
[42]Zhao, X., J. Si, D. Huang, K. Li, Y. Xin, and M. Sui. Application of star poly(ethylene glycol) derivatives in drug delivery and controlled release. *J. Control Release*. 323:565–577, 2020. https://doi.org/10.1016/j.jconrel.2020.04.039.